

## An integrated microfluidic platform for quantifying drug permeation across biomimetic vesicle membranes

Michael Schaich, Jehangir Cama, Kareem Al Nahas, Diana Sobota, Hannah Sleath, Kevin Jahnke, Siddharth Deshpande, Cees Dekker, and Ulrich F Keyser

*Mol. Pharmaceutics*, **Just Accepted Manuscript** • DOI: 10.1021/acs.molpharmaceut.9b00086 • Publication Date (Web): 17 Apr 2019

Downloaded from <http://pubs.acs.org> on April 18, 2019

### Just Accepted

“Just Accepted” manuscripts have been peer-reviewed and accepted for publication. They are posted online prior to technical editing, formatting for publication and author proofing. The American Chemical Society provides “Just Accepted” as a service to the research community to expedite the dissemination of scientific material as soon as possible after acceptance. “Just Accepted” manuscripts appear in full in PDF format accompanied by an HTML abstract. “Just Accepted” manuscripts have been fully peer reviewed, but should not be considered the official version of record. They are citable by the Digital Object Identifier (DOI®). “Just Accepted” is an optional service offered to authors. Therefore, the “Just Accepted” Web site may not include all articles that will be published in the journal. After a manuscript is technically edited and formatted, it will be removed from the “Just Accepted” Web site and published as an ASAP article. Note that technical editing may introduce minor changes to the manuscript text and/or graphics which could affect content, and all legal disclaimers and ethical guidelines that apply to the journal pertain. ACS cannot be held responsible for errors or consequences arising from the use of information contained in these “Just Accepted” manuscripts.



1  
2  
3  
4  
5  
6  
7 An integrated microfluidic platform for quantifying  
8  
9  
10  
11 drug permeation across biomimetic vesicle  
12  
13  
14  
15 membranes  
16  
17  
18  
19

20 *Michael Schaich<sup>1</sup>, Jehangir Cama<sup>1,2</sup>, Kareem Al Nahas<sup>1</sup>, Diana Sobota<sup>1</sup>, Hannah Sleath<sup>1</sup>,*  
21 *Kevin Jahnke<sup>1,3,4</sup>, Siddharth Deshpande<sup>5</sup>, Cees Dekker<sup>5</sup>, Ulrich F. Keyser<sup>1</sup>*  
22  
23

24  
25  
26 <sup>1</sup> Cavendish Laboratory, University of Cambridge, JJ Thomson Avenue, Cambridge, CB3 0HE,  
27  
28 United Kingdom  
29

30  
31 <sup>2</sup> Living Systems Institute, University of Exeter, Stocker Road, Exeter, EX4 4QD, United  
32  
33 Kingdom  
34

35  
36  
37 <sup>3</sup> Department of Biophysical Chemistry, University of Heidelberg, Im Neuenheimer Feld 253,  
38  
39 D-69120, Heidelberg, Germany  
40

41  
42 <sup>4</sup> Max Planck Institute for Medical Research, Department of Cellular Biophysics, Jahnstraße 29,  
43  
44 D-69120, Heidelberg, Germany  
45

46  
47  
48 <sup>5</sup> Department of Bionanoscience, Kavli Institute of Nanoscience, Delft University of Technology,  
49  
50 Van der Maasweg 9, 2629 HZ Delft, The Netherlands  
51

## Keywords

Microfluidics, Lab on chip, Liposomes, GUV, Antibiotics, Drug transport, Permeability

## Abstract

The low membrane permeability of candidate drug molecules is a major challenge in drug development and insufficient permeability is one reason for the failure of antibiotic treatment against bacteria. Quantifying drug transport across specific pathways in living systems is challenging since one typically lacks knowledge of the exact lipidome and proteome of the individual cells under investigation. Here, we quantify drug permeability across biomimetic liposome membranes, with comprehensive control over membrane composition. We integrate the microfluidic octanol-assisted liposome assembly platform with an optofluidic transport assay to create a complete microfluidic total analysis system for quantifying drug permeability. Our system enables us to form liposomes with charged lipids mimicking the negative charge of bacterial membranes at physiological pH and salt concentrations, which proved difficult with previous liposome formation techniques. Furthermore, the microfluidic technique yields an order of magnitude more liposomes per experiment than previous assays. We demonstrate the feasibility of the assay by determining the permeability coefficient of norfloxacin and ciprofloxacin across biomimetic liposomes.

## I. Introduction

Over the past decades, multidrug resistance (MDR) in microbial pathogens has developed into a serious threat for public health, leading to a global medical crisis<sup>1</sup>. In 2016, more than half (58.6%) of clinical *Escherichia coli* isolates in the European Union showed resistance to at least one of the antimicrobial groups under regular surveillance<sup>2</sup>. One of the major biochemical causes of antibiotic resistance is the reduced membrane permeability of drug molecules<sup>3-6</sup>. This problem is especially apparent for Gram-negative bacteria, as their cell envelope consists of a double membrane; drugs require seemingly contradictory chemical properties to overcome these two barriers to reach their cytoplasmic targets<sup>4,6,7</sup>. A deeper understanding of the mechanisms that govern passive drug transport across lipid membranes is therefore of great importance.

Bacterial cell membranes are very complex systems that are involved in numerous cellular processes<sup>8</sup>. Drug permeability studies have not only proven very difficult due to the small size of the bacteria, but also due to the convolution of active and passive effects that simultaneously take place in the membranes of living bacteria<sup>6,9</sup>. Many studies on membrane properties are therefore performed using lipid vesicles (or liposomes) as model systems<sup>9</sup>. Liposomes of several microns in size, referred to as giant unilamellar vesicles (GUVs), offer the advantages of having well-defined lipid compositions, being easy to image and also being more controlled systems for studying transport processes than a living bacterium. Due to these advantages, liposomes have been the subject of intensive research and their applications now reach far beyond the drug delivery<sup>10</sup> and synthetic biology communities<sup>11-13</sup>.

Various methods to produce lipid vesicles have been developed<sup>14</sup>. Albeit offering good control over lipid composition, many technologies such as electroformation suffer from drawbacks such as low yield, batch-to-batch variability, low encapsulation efficiency and polydispersity; these

1  
2  
3 problems are especially acute at high salt concentrations and when using charged lipids<sup>15</sup>.  
4  
5 Microfluidic methods to form liposomes can overcome these limitations, but often require oil as  
6  
7 the lipid carrying solvent, which must be removed in further procedures<sup>16</sup>. The recently developed  
8  
9 microfluidic technique octanol-assisted liposome assembly (OLA) replaces the oil phase with the  
10  
11 aliphatic alcohol 1-octanol<sup>17</sup>. A double emulsion of water in octanol self-assembles into a liposome  
12  
13 with an octanol pocket attached to it upon production. The octanol pocket later pinches off within  
14  
15 a few minutes, resulting in a liposome and a separated octanol droplet.  
16  
17  
18

19 We have previously presented an optofluidic permeability assay which allows us to determine  
20  
21 the permeability coefficient of electroformed GUVs to fluoroquinolone drugs in a direct, label-  
22  
23 free manner<sup>18</sup>. The assay exploits the autofluorescence property of fluoroquinolones in the  
24  
25 ultraviolet for label-free detection. GUVs are exposed to a drug solute in a controlled manner in a  
26  
27 microfluidic device. We use ultraviolet video fluorescence microscopy to quantify drug uptake in  
28  
29 the GUVs and report the permeability coefficient of the drug across the membrane composition of  
30  
31 interest. We used this method to show the influence of lipid composition on fluoroquinolone  
32  
33 transport<sup>19</sup>. Furthermore, we showed that the permeability of different drugs from the  
34  
35 fluoroquinolone family can span over two orders of magnitude at different pH levels<sup>20</sup>. Finally, we  
36  
37 used the assay to study the transport behavior of proteoliposomes containing the *E. coli* outer  
38  
39 membrane protein OmpF<sup>21</sup>, thus developing a direct, optical measurement for antibiotic flux  
40  
41 through porins, which form an important route for drug molecules to translocate across the outer  
42  
43 membrane of Gram-negative bacteria<sup>5</sup>.  
44  
45  
46  
47  
48

49 Despite these advances, the technique suffered from the various drawbacks of off-chip liposome  
50  
51 formation described above. In this paper, we present the successful integration of the OLA  
52  
53 platform with our optofluidic transport assay. This lab-on-chip total analysis platform enables the  
54  
55  
56  
57  
58  
59  
60

1  
2  
3 continuous production and screening of liposomes on the same device. This enabled us to  
4  
5 efficiently screen an order of magnitude more liposomes than in our earlier platform. Importantly,  
6  
7 it also enables us to explore transport using physiological salt concentrations which was  
8  
9 challenging using electroformed GUVs<sup>22</sup>. We also present an improved MATLAB analysis  
10  
11 routine, which offers superior liposome detection, automatic channel recognition and more  
12  
13 debugging options than our earlier platform. The method was validated by performing transport  
14  
15 experiments of the fluoroquinolone drugs norfloxacin and ciprofloxacin through biomimetic  
16  
17 PGPC liposomal membranes. We verified that the liposomes produced are indeed unilamellar by  
18  
19 performing a dithionite bleaching assay.  
20  
21  
22  
23  
24  
25  
26  
27  
28  
29  
30  
31  
32  
33  
34  
35  
36  
37  
38  
39  
40  
41  
42  
43  
44  
45  
46  
47  
48  
49  
50  
51  
52  
53  
54  
55  
56  
57  
58  
59  
60

## II. Materials and Methods

### Microfluidic Chip Design

The microfluidic device integrates the channel features used for octanol-assisted liposome assembly (OLA) with a downstream T-junction geometry to form a complete lab-on-chip system for the continuous production and screening of liposomes. A schematic of the device is shown in Fig 1A.

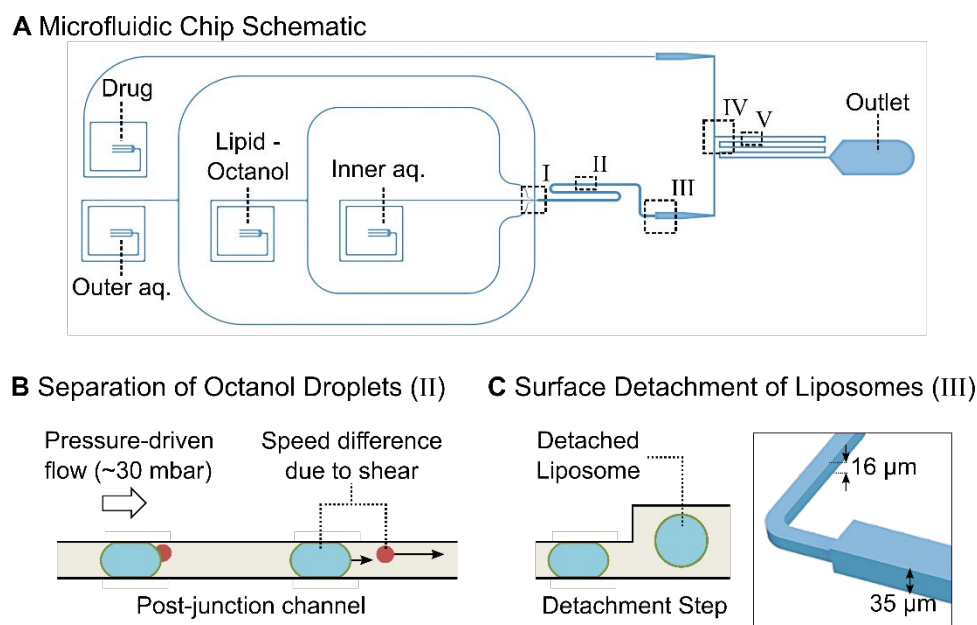


**Figure 1.** Microfluidic total analysis system for quantifying drug permeability across liposome membranes. A: The microfluidic chip features four inlets, one outlet and two different channel heights. The outer aqueous, inner aqueous and lipid-octanol inlets are needed for liposome production on chip. The fourth inlet is used to flush in the drug whose permeability is to be measured. The liposome production occurs at a 6-way junction, where the aqueous flows meet the lipid-octanol phase (I). The 1-octanol pocket which is initially attached to the liposome separates from it in the post-junction channel within minutes after production (II). After an increase in channel height (III), the liposomes are mixed with the drug solute (IV). The transport measurement

1  
2  
3 takes place as the liposomes flow towards the outlet, immersed in a bath of the autofluorescing  
4 drug (V). B: Mechanism to separate the liposome population from the octanol droplets. The  
5 liposomes typically have radii of 15-18  $\mu\text{m}$  upon production and octanol droplets of  $< 8 \mu\text{m}$ . The  
6 channel height post formation is lower than the diameter of the liposomes which leads to a  
7 significant difference in velocity for octanol droplets and liposomes as indicated by the arrows.  
8 The octanol droplets pass through the device first and are discarded at the outlet. C: Upon  
9 production, the liposomes' diameters are larger than the height of the microfluidic channel. An  
10 increase in channel height from 16  $\mu\text{m}$  to 35  $\mu\text{m}$  frees the liposomes from the geometric  
11 confinement and enables transport measurements across the membrane without the risk of shear-  
12 induced leakage.  
13  
14  
15  
16  
17  
18  
19  
20  
21  
22  
23  
24  
25  
26  
27  
28

29 The 6-way junction where the liposomes are created is shown in Fig. 2A. The design of the  
30 junction enables the formation of double-emulsion droplets. This leads to the production of a lipid  
31 bilayer encapsulating an aqueous compartment with a 1-octanol pocket attached to it. The octanol  
32 droplet then buds off the liposome due to a combined effect of surface energy minimization and  
33 shear stress induced by the surrounding fluid streams, as well as contact with the channel wall<sup>17</sup>.  
34 The original design geometry<sup>17</sup> was modified to fit the needs of the drug transport assay. The  
35 dimensions of the junction were scaled up by a factor of 2 to achieve liposome diameters of up to  
36 35  $\mu\text{m}$ . The larger channels furthermore lead to higher flow rates and higher liposome production  
37 rates. A side effect of the larger liposomes and the altered flow conditions is that the budding off  
38 of the octanol pocket from the liposomes requires more time than for smaller vesicles. The budding  
39 off process has previously been reported to occur within a minute after production<sup>23</sup>, whereas this  
40 process is on the time scale of minutes using our chip geometry.  
41  
42  
43  
44  
45  
46  
47  
48  
49  
50  
51  
52  
53  
54  
55  
56  
57  
58  
59  
60



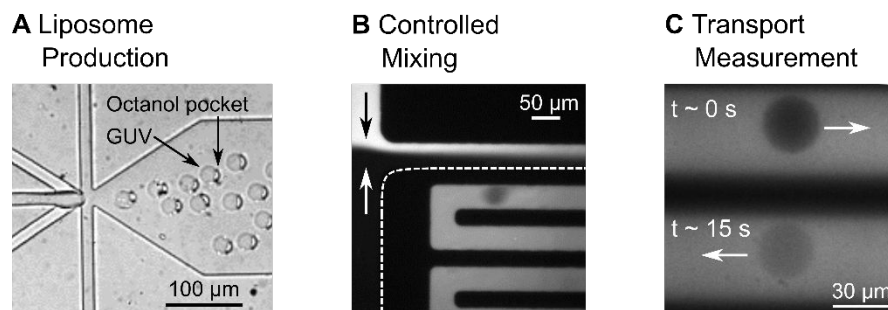


**Figure 2.** Liposomes at different positions in the microfluidic chip. A: Liposome assembly at the 6 way formation junction. A 1-octanol pocket is initially attached to the liposomes. The liposome and the octanol pocket separate further downstream in the post-junction channel. B: The liposomes experience a spontaneous exposure to a drug solute at a T-junction where the two flows mix in a controlled manner. C: The liposomes, surrounded by the autofluorescing drug ( $\lambda_{\text{ex}} = 350 \text{ nm}$ ), can be monitored at different parts of the channel, corresponding to different times that the liposome has been exposed to the drug. The increase in liposome intensity as the fluorescing drug diffuses across the membrane is used to determine the permeability coefficient of the drug across the lipid membrane under investigation.

The generated liposomes have diameters larger than the height of the post-junction channel. These liposomes therefore initially shear along the PDMS walls, as they flow downstream. To ensure that the shear does not compromise the membranes during the subsequent transport measurements, an increment in channel height was introduced, increasing the channel height from 16  $\mu\text{m}$  to 35  $\mu\text{m}$  (Fig. 1C). Post the step, the liposomes flow towards the mixing junction without shearing.

Reaching the T-junction, the liposomes are exposed to a drug solute as they flow towards the outlet channel (Fig. 2B). Drug transport across the liposome membrane is tracked label-free by

1  
2  
3 exploiting the autofluorescence of the drug in the UV region ( $\lambda_{\text{ex}} = 350$  nm). The liposomes  
4 initially appear dark on a bright background due to the lack of fluorescent drug molecules within  
5 them. As the fluorescent drug molecules diffuse through the membrane, the liposomes get brighter,  
6 as seen in Fig. 2C. We record and analyze the increase in fluorescence intensity using a previously  
7 established analytical protocol to quantify the permeability coefficient of the drug molecule for the  
8 specific lipid composition under investigation<sup>18,20</sup>.  
9  
10  
11  
12  
13  
14  
15  
16  
17  
18

### 19 **Separation of Octanol Droplets and Liposomes Based on Flow Speed**

20  
21 The shearing of the liposomes in the post-junction channel is exploited to separate the liposome  
22 population from the octanol droplets. This separation mechanism, visualized in Fig. 1B, is based  
23 on the difference in flow speeds between the liposomes and the droplets. Upon production, the  
24 liposomes typically have radii of 15-18  $\mu\text{m}$ , whereas the octanol droplets have radii of under 8  $\mu\text{m}$ .  
25 The channel height of 16  $\mu\text{m}$  before the step causes deformation and shearing of the liposomes  
26 with the PDMS and slows their flow speed down considerably. In comparison, the smaller octanol  
27 droplets do not shear and therefore possess a higher velocity. Liposomes typically move with  
28 speeds of  $\sim 0.05$  mm/s, whereas the droplets move at  $\sim 0.2$  mm/s in this region of the chip. We fill  
29 the post formation channel with the required number of liposomes and subsequently terminate  
30 liposome formation by reducing the aqueous flows (IA and OA) and stopping the lipid-octanol  
31 flow (LO) completely. The smaller octanol droplets in the channel get flushed through the mixing  
32 junction and out of the chip before the larger liposomes reach the junction; the process is possible  
33 since the surface interactions result in different flow speeds of the liposomes and smaller octanol  
34 droplets (Fig. 1B). The velocity difference explains the observed separation of the octanol droplets  
35 and liposomes on chip. After reaching the step, the liposomes are no longer pressed against the  
36  
37  
38  
39  
40  
41  
42  
43  
44  
45  
46  
47  
48  
49  
50  
51  
52  
53  
54  
55  
56  
57  
58  
59  
60

1  
2  
3 channel walls, reconfigure to an expected isotropic spherical geometry and encounter the drug  
4  
5 flow at the T-junction.  
6  
7  
8  
9

## 10 **Chip Fabrication**

11  
12 The microfluidic chips are made of polydimethylsiloxane (PDMS) using established photo- and  
13  
14 soft- lithography techniques. The master mold is generated by spin coating a thin layer of SU-8  
15  
16 2025 photoresist (Chestech, UK) on a 4-inch Silicon wafer (University Wafer, USA). The wafer  
17  
18 is pre-baked on a hot plate at 65°C for 1 min and at 95°C for 6 min. The structures are imprinted  
19  
20 on the substrate using a table-top laser direct imaging (LDI) system (LPKF ProtoLaser LDI,  
21  
22 Germany). The LDI system exposes the structures specified in the software directly with UV light,  
23  
24 causing the photoresist to crosslink and solidify. After exposure, the wafer is post-baked for 1 min  
25  
26 at 65°C and for 6 min at 95°C. The substrate is developed by rinsing the wafer with propylene  
27  
28 glycol monomethyl ether acetate (PGMEA), which removes the unexposed photoresist and leaves  
29  
30 the desired UV-exposed structures on the substrate. The wafer is then hard baked for 15 min at  
31  
32 120°C. The multi-height feature is achieved by performing this photo-lithography process twice  
33  
34 on the same silicon wafer with different layers of photoresist with varying heights. Feature heights  
35  
36 of 16  $\mu\text{m}$  and 35  $\mu\text{m}$  respectively were obtained by spinning the photoresist at 3800 rpm and 1800  
37  
38 rpm respectively (WS-650-23NPP, Laurell Technologies, USA) for 60 s with a ramp of 100 rpm/s.  
39  
40 The anchoring tool of the direct laser writer is used for aligning the features in the two designs.  
41  
42  
43  
44  
45

46  
47 The PDMS microfluidic devices are made by using the silicon master as a mold. Liquid PDMS  
48  
49 (Sylgard 184, Dow Corning) is mixed in a 9:1 ratio with the curing agent and desiccated to remove  
50  
51 air bubbles. It is then cast into the mold and cured for 60 min at 60°C. Fluid access ports of  
52  
53 0.75 mm diameter for the inlets and 1.5 mm diameter for the outlet are punched into the chip using  
54  
55  
56  
57  
58  
59  
60

1  
2  
3 biopsy punches (WPI, UK). The PDMS chip is then plasma-bonded to PDMS-coated cover slips  
4  
5 using a standard plasma bonding protocol (100 W, 10 s exposure, 25 sccm, plasma oven from  
6  
7 Diener Electric, Germany).  
8  
9

10 The surfaces of the outlet channel are rendered hydrophilic by flushing the channel with a  
11  
12 polyvinyl alcohol (PVA) solution for 15 min (50 mg/mL, 87-90% hydrolysed molecular weight  
13  
14 30,000-70,000 Da, Sigma-Aldrich) via the outer aqueous inlet, using a previously established  
15  
16 protocol<sup>17</sup>. Post treatment, the PVA is removed from the channels by applying suction with a  
17  
18 vacuum pump (Gardner Denver Thomas GmbH, Germany) after which the microfluidic device is  
19  
20 baked in the oven at 120°C for 15 min.  
21  
22  
23  
24  
25

## 26 **Optical Setup**

27  
28 The microfluidic chips are either run on a custom-built UV epifluorescence setup, or on a  
29  
30 commercial epifluorescence microscope (Nikon TE 2000U) to induce autofluorescence in the drug  
31  
32 molecules and to capture the experimental video data. In the custom built setup, white light from  
33  
34 a broadband light source (EQ99FC, Energetiq, USA) enters a monochromator (Monoscan 2000,  
35  
36 OceanOptics, USA) where the excitation wavelength ( $\lambda_{\text{ex}} = 350 \text{ nm}$ ) for the target drug molecule  
37  
38 is selected. The UV light passes through a Köhler illumination pathway and illuminates the  
39  
40 microfluidic device via a quad band dichroic mirror (BrightLine full-multiband filter set, Semrock,  
41  
42 USA) and a microscope objective. The fluorescence signal is detected by an EMCCD camera  
43  
44 (Evolve 512 Delta, Photometrics). The camera and recording settings (exposure 10 ms, bin 2,  
45  
46 gain 150) are controlled using the open source software  $\mu$ Manager 1.4<sup>24</sup>. A 60 $\times$  water immersion  
47  
48 objective (UPLSAPO NA 1.2, Olympus) is used for data recording, whereas lower magnifications  
49  
50 (4 $\times$ , 10 $\times$ , 20 $\times$ , Plan Achromat, Olympus) are used for optimizing the vesicle formation and PVA  
51  
52  
53  
54  
55  
56  
57  
58  
59  
60

1  
2  
3 treatment of the chip. The Nikon epifluorescence microscope is equipped with a pE-1 LED lamp  
4  
5 ( $\lambda_{\text{ex}} = 365 \text{ nm}$  (DAPI), Cool LED, UK) and uses the same water immersion objective, dichroic  
6  
7 mirror and camera (exposure 15 ms, bin 2, gain 250) as the custom built setup.  
8  
9

## 10 11 12 **Solution Compositions and Flow Control** 13

14  
15 The base solutions for the OLA aqueous phases consist of 200 mM sucrose and 15% v/v glycerol  
16  
17 in buffer. In accordance to previously published protocols, the outer aqueous phase additionally  
18  
19 contains 50 mg/mL poloxamer Kolliphor P-188, which facilitates the initial double-emulsion  
20  
21 formation<sup>23</sup>. We performed experiments on the fluoroquinolone drugs norfloxacin and  
22  
23 ciprofloxacin. Transport of both drugs is measured in phosphate-buffered saline (pH 7.4) which  
24  
25 mimics physiological pH and salt concentrations. Additionally, experiments using a 5 mM acetic  
26  
27 acid buffer (pH 5) are performed for norfloxacin as controls for membrane stability. At pH 5,  
28  
29 norfloxacin molecules are primarily in their positively charged form and hence show low  
30  
31 permeability through lipid bilayers<sup>18,20</sup>. The drug solutes are prepared by diluting 48.5 mM  
32  
33 norfloxacin and 49.5 mM ciprofloxacin stock solutions, respectively, to a final concentration of  
34  
35 2 mM with the aqueous base stock. All pH levels are adjusted and checked using a digital pH meter  
36  
37 (Hanna Instruments, UK). The lipid-octanol phase is obtained by dissolving a 100 mg/mL lipid  
38  
39 stock mixture with 1-octanol to reach a final concentration of 2 mg/mL. The lipid stock is a 3:1  
40  
41 mixture of DOPC (1,2-dioleoyl-sn-glycero-3-phosphocholine) and DOPG (1,2-Dioleoyl-sn-  
42  
43 glycero-3-phosphorac-(1-glycerol) sodium salt) in 100% Ethanol. DOPG is an anionic lipid with  
44  
45 a net charge of -1. Lipid mixtures of DOPG with the net-charge neutral lipid DOPC roughly mimic  
46  
47 the negative charge density of bacterial lipid extracts and are typically used when modelling  
48  
49  
50  
51  
52  
53  
54  
55  
56  
57  
58  
59  
60

1  
2  
3 bacterial membranes with GUVs<sup>25–28</sup>. All chemicals are obtained from Sigma-Aldrich, unless  
4  
5 stated otherwise.  
6

7  
8 The liquid flows in the microfluidic device are controlled with a pressure-driven microfluidic  
9  
10 pump (MFCS-EZ, Fluigent). The fluids are stored in Fluiwell-4C reservoirs (Micrewtube 0.5mL,  
11  
12 Simport) and enter the microfluidic chip via a polymer tubing (Tygon microbore tubing, 0.020’’ x  
13  
14 0.060’’ OD, Cole Parmer). Cut dispensing tips (Gauge 23 blunt end, Intertronics) are used as metal  
15  
16 connectors between the tubing and the chip.  
17  
18  
19  
20

## 21 **Experimental Protocol**

22  
23  
24 The microfluidic assay involves a 2-stage protocol. The first stage involves adjusting the  
25  
26 pressure-driven flows of the liquids to obtain stable liposome production, as reported previously<sup>17</sup>.  
27  
28 Typically, pressures of ~40 mbar for the inner aqueous, lipid-octanol and drug inlet phases, and  
29  
30 ~70 mbar for the outer aqueous phases lead to a stable production of liposomes. After the post-  
31  
32 formation channel has been typically filled with hundreds of liposomes, the aqueous flows are  
33  
34 reduced (IA and OA input pressures at this stage are typically reduced to around 15 mbar each),  
35  
36 and the lipid-octanol flow is stopped completely. Due to the difference in flow speeds described  
37  
38 in Fig. 1B, the octanol droplets flow out of the chip leaving a population of octanol free liposomes  
39  
40 in the post-formation channel. Throughout the entire process the T-junction is regularly monitored  
41  
42 in the post-formation channel. Throughout the entire process the T-junction is regularly monitored  
43  
44 to ensure that the drug and OLA flows mix equally and that no octanol enters the drug channel.  
45  
46

47  
48 The next stage involves the drug permeability measurement, using the same measurement  
49  
50 principles previously employed in our laboratory<sup>18–21</sup>. The field-of-view is changed to the channel  
51  
52 network post the T-junction, shortly after the liposomes encounter the drug flow (Fig. 2C). Using  
53  
54 a 60× water immersion objective (UPLSAPO, NA 1.2, Olympus), two sections of the channel are  
55  
56  
57  
58  
59  
60

1  
2  
3 monitored simultaneously with sufficient resolution to study the transport process. Since the  
4 liposome is dispensed in the drug solution flowing along the channel, the different positions in the  
5 channel correspond to different drug exposure times of the liposome. The IA and OA pressures  
6 are maintained at 15 mbar each, resulting in flow speeds in the channel of about 0.5 mm/s. One  
7 measurement is taken just after the drug and the vesicle flows meet ( $t \approx 0$  s), the other one typically  
8 after the liposomes have been exposed to the drug for  $\sim 15$  seconds. Measurements of up to 40  
9 seconds of drug exposure can be obtained at these flow rates by recording the liposomes at the end  
10 of the channel network, just before the outlet reservoir. This can be further increased by increasing  
11 the length of the mixing channel<sup>18</sup>.

12  
13  
14  
15  
16  
17  
18  
19  
20  
21  
22  
23  
24 After all the liposomes have been flushed through, the liposome formation can be restarted, and  
25 the experiment repeated. The number of repeats is limited by the quality of the PVA coating and/or  
26 accumulation of lipid and octanol aggregates in the chip. The data presented here was obtained by  
27 performing up to four such repeats on a single chip. However, more repeats are possible and we  
28 managed to use a chip to perform up to 11 experiments consecutively. Generally, OLA allows for  
29 continuous liposome production with a frequency of up to 100 Hz for several hours<sup>23</sup>.

### 30 31 32 33 34 35 36 37 38 39 40 **Data Processing and Permeability Calculation**

41  
42 The data is analyzed using our previously established permeability model<sup>18–20</sup>. The videos  
43 obtained are processed using a MATLAB routine. Similar to our previously reported analysis  
44 routine, the script extracts the radius, the speed, the circularity and the intensity values of the  
45 liposomes passing through the channels. We have updated the image analysis routine, which now  
46 additionally features superior liposome detection, automatic channel recognition and debugging  
47 options that are explained in detail in the Supplementary Information.

1  
2  
3 The permeability coefficient is obtained by the equation<sup>18</sup>:  
4

$$5 \quad P = -\left(\frac{R}{3t}\right) \times \ln(\Delta I(t) - \Delta I(0) + 1)$$

6  
7  
8  
9 Where the variable R is the radius of the liposome, t is the time of its exposure to the antibiotic  
10 and  $\Delta I$  is the normalized autofluorescence intensity difference between the interior ( $I_{in}$ ) and the  
11 exterior ( $I_{out}$ ) of the liposome:  
12  
13  
14

$$15 \quad \Delta I = \frac{I_{out} - I_{in}}{I_{out}}$$

16  
17  
18  
19  
20  
21  
22 The difference in the normalized intensity of the liposomes at different drug exposure times can  
23 be used as a direct readout of drug flux into the liposomes<sup>18</sup>. Due to the initial lack of fluorescing  
24 drug molecules inside the liposome,  $\Delta I(t = 0)$  has a high value, correlating to a large difference  
25 in fluorescence intensity between the liposome ( $I_{in}$ ) and the background ( $I_{out}$ ). In contrast,  $\Delta I(t)$   
26 at the later time point has a lower value consistent to a lower difference in fluorescence intensity  
27 between the liposome and the background, due to the influx of fluorescing drug molecules. Further  
28 explanations and a derivation of the Equations have been published in our previous work<sup>18,20</sup>.  
29  
30  
31  
32  
33  
34  
35  
36  
37  
38  
39  
40  
41  
42  
43  
44  
45  
46  
47  
48  
49  
50  
51  
52  
53  
54  
55  
56  
57  
58  
59  
60



### III. Results

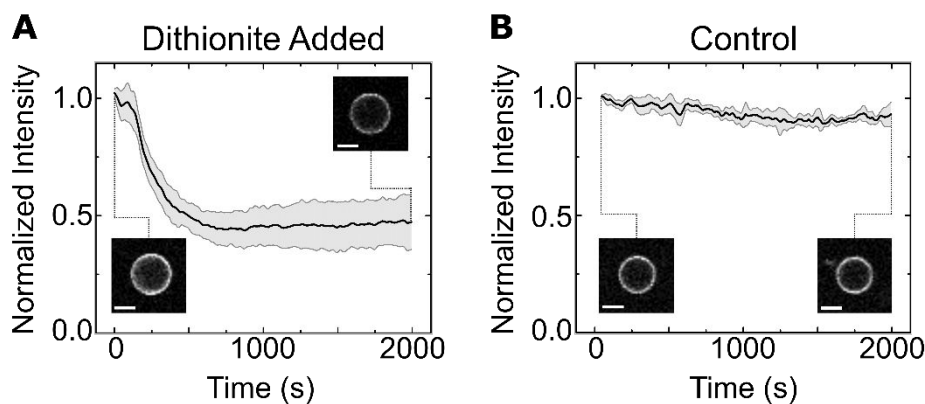
#### Test for Membrane Unilamellarity

Liposomes produced by OLA have previously been tested for their unilamellarity via the incorporation of the pore forming toxin  $\alpha$ -hemolysin<sup>17</sup>. Additionally, the antimicrobial peptide cecropin B was found to permeabilize and lyse OLA-produced liposomes, again suggesting that the liposomes are unilamellar<sup>28</sup>. As an additional, quantitative technique to verify the unilamellarity of the OLA-produced liposomes, we extracted the liposomes from our microfluidic device and subjected them to a dithionite bleaching assay. If brought in contact with it, the membrane-impermeable anion dithionite reduces and thereby irreversibly bleaches nitrobenzoxadiazole (NBD). By subjecting unilamellar liposomes containing NBD-labelled lipids to a dithionite solution, the fluorescence intensity of the liposome drops to half of the initial value, due to the bleaching of the outer leaflet of the bilayer membrane<sup>29,30</sup>.

The composition of the inner and outer aqueous solutions used for liposome production in this experiment is identical to the solutions of the drug transport assay described above. The lipid-octanol phase additionally contains 0.01 mg/mL of a fluorescently labelled NBD-PC lipid (1-palmitoyl-2-{6-[(7-nitro-2-1,3-benzoxadiazol-4-yl) amino] hexanoyl}-sn-glycero-3-phosphocholine, Avanti Polar Lipids, USA). A standard PDMS chip with the design shown in Fig. 1 is used to extract the liposomes off chip. However, instead of applying a  $\varnothing$  1.5 mm punch at the outlet, a  $\varnothing$  4 mm hole is punched at the detachment step in this case. The  $\varnothing$  4 mm outlet serves as a fluid reservoir where the liposomes are collected. After the pressures of the microfluidic pump have been adjusted to achieve a stable liposome production, an additional 20  $\mu$ l of the IA solution is pipetted into the reservoir, which aids the separation of liposomes and octanol droplets in the reservoir. Due to the lower density of octanol, the droplets rise to the surface of the reservoir.

1  
2  
3 A larger fluid volume furthermore facilitates liposome extraction. After 1 hour of liposome  
4 production, 15  $\mu\text{l}$  of the liposome suspension is extracted from the reservoir using a wide bore  
5 pipette tip.  
6  
7  
8  
9

10 The liposome suspension is added to a microscopy chamber (Grace Bio-Labs FlexWell™,  
11 Sigma Aldrich) on a BSA-coated coverslip containing 35  $\mu\text{l}$  of a solution containing PBS, 200 mM  
12 glucose and 15% v/v glycerol. The liposomes are left for 1 hour to sink and settle at the bottom of  
13 the chamber which facilitates imaging. A dithionite solution stock (1M sodium dithionite in Tris  
14 pH 10 buffer, Sigma Aldrich) is diluted in the glucose buffer to a final dithionite concentration of  
15 15 mM. 30  $\mu\text{l}$  of the solution is added to the liposome suspension after the imaging is started<sup>30</sup>.  
16  
17 Imaging is performed on a confocal microscope (Olympus IX83, FV10-MCPSU laser system, 20x  
18 objective UPLSAPO Olympus, 5 s frame interval). Image analysis is performed using the open  
19 source software Image J.  
20  
21  
22  
23  
24  
25  
26  
27  
28  
29



45 **Figure 3.** Normalized intensity traces of the liposome membranes. A: Intensity drop of the  
46 liposome membranes (N = 10) upon addition of dithionite. The mean intensity of the observed  
47 liposomes is shown in black with the standard deviations depicted in grey. The drop to half of the  
48 initial value is caused by the bleaching of the outer membrane leaflet by the dithionite.  
49  
50  
51  
52  
53  
54 B: Liposome intensity (N = 3) stays stable throughout the entire experiment upon addition of buffer  
55  
56  
57  
58  
59  
60

1  
2  
3 without dithionite, suggesting a negligible effect of photo bleaching. The insets show a  
4 representative liposome at the beginning of the measurement and after 2000 s. The scale bar shows  
5  
6  
7  
8 10  $\mu\text{m}$ .  
9

10  
11  
12  
13 The intensity traces of the liposomes normalized to their initial intensity value are depicted in  
14 Figure 3. Fig. 3A shows the intensity drop upon addition of dithionite, whereas Fig. 3B shows the  
15 results of the bleaching control experiment upon addition of buffer without dithionite. The mean  
16 intensity of the observed liposomes is shown as black line with the standard deviations depicted in  
17 grey. The intensity of the liposomes subjected to dithionite ( $N = 10$ ) drops to half of the initial  
18 intensity after about 500 seconds and then stays steady at that value. These results suggest that the  
19 liposomes indeed consist of a single lipid bilayer, whose outer leaflet is bleached by the  
20 dithionite<sup>29</sup>. Since the dithionite anion cannot penetrate the membrane, the inner leaflet of the  
21 membrane is not affected by the dithionite and remains fluorescent. The control experiment  
22 without dithionite in Fig 3B shows a stable intensity signal over the timespan of the entire  
23 experiment ( $N = 3$ ). This suggests that photo bleaching does not play a significant role in the  
24 observed drop in the intensity and that we are indeed observing the bleaching of the outer leaflet  
25 of a single bilayer.  
26  
27  
28  
29  
30  
31  
32  
33  
34  
35  
36  
37  
38  
39  
40  
41  
42  
43  
44

### 45 **Passive Diffusion Measurements**

46  
47 Norfloxacin transport measurements were performed in two different chemical environments.  
48 One set of measurements was performed at physiological pH and salt concentrations (PBS). The  
49 second set was taken as a control in an acetic acid buffer at pH 5. The majority of norfloxacin  
50 molecules are positively charged at pH 5 whereas the proportion of uncharged molecules is  
51  
52  
53  
54  
55  
56  
57  
58  
59  
60

increased at pH 7.4<sup>18,20,21,31</sup>. The liposomes consisted of PCPG lipids in a 3:1 ratio, a mixture which is commonly used as a model for bacterial membranes due to its negative charge<sup>25,26</sup>.

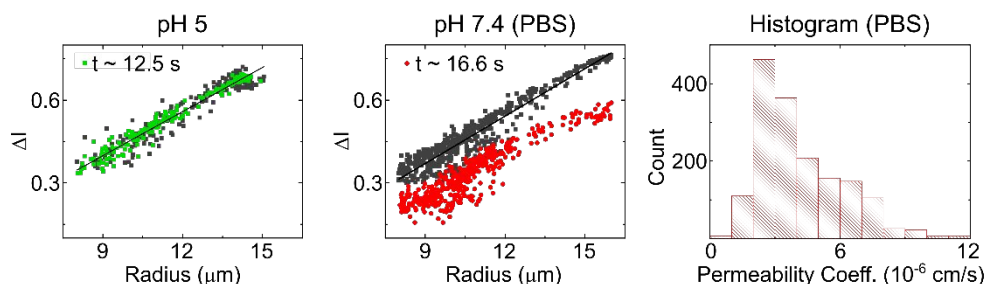


**Figure 4.** Norfloxacin diffusion experiments across PCPG liposomal membranes. The scatterplots show representative drug uptake experiments at pH 5 and pH 7.4, respectively. Each point in the scatter plots corresponds to the measured normalized intensity difference of a liposome. The dark points are obtained at  $t \approx 0$ , just after the liposomes encounter the drug flow. The colored points show the value at the second measurement position, after exposure to the drug for the time indicated in the panel. The gap between the black and red points for the measurement in PBS indicates norfloxacin membrane permeability. The histogram shows the distribution of all permeability measurements combined at pH 7.4 ( $N = 1620$ , 5 technical repeats). The distribution has a mean value of  $4.13 \pm 0.05 \times 10^{-6}$  cm/s (mean  $\pm$  std. error of mean) and a median value of  $3.57 \times 10^{-6}$  cm/s.

The scatter plots in Fig. 4 show representative results from such experiments. The black data points mark the normalized intensity difference levels  $\Delta I(0)$  of individual liposomes at the first measurement point, when the liposomes have just encountered the drug flow and hence do not contain any drug molecules within them. The colored data points mark the normalized intensity difference  $\Delta I(t)$  of the individual liposomes after they have been exposed to the drug for the time

1  
2  
3 indicated inset. The liposomes in PBS show a substantial drop in  $\Delta I$  after being exposed to the  
4 drug, whereas the measurements at the different time points overlap when the studies are  
5 conducted at pH 5.  
6  
7  
8  
9

10 Since the drop in  $\Delta I$  is a direct result of the influx of fluorescent molecules, we can conclude  
11 that no significant transport occurs at pH 5 over the observed timespans, whereas there is  
12 substantial norfloxacin transport at physiological pH and salt concentrations. The technical repeats  
13 of this experiment shown in Fig. S3 and Fig. S4 (ESI) report similar results. Expanding the  
14 exposure and observation time for the pH 5 measurement to 40 seconds yields the same result of  
15 no significant transport, in line with our previous observations. This also confirms that the  
16 liposome membranes are not being compromised due to shear or any other interactions in our  
17 device.  
18  
19  
20  
21  
22  
23  
24  
25  
26  
27

28 The observed transport behavior is to be expected, as the norfloxacin molecule is predominantly  
29 uncharged or zwitterionic at neutral pH, whereas the molecule is in a charged state at pH 5<sup>32</sup>. Lipid  
30 membranes are generally regarded as largely impermeable to ions and highly charged molecules,  
31 since these cannot cross the hydrocarbon section of the lipid bilayer easily. In nature, these  
32 transport processes are governed by transmembrane proteins such as porins or ion channels<sup>33</sup>.  
33  
34  
35  
36  
37  
38  
39

40 The spread in vesicle radius observed in Fig. 4 is a result of the method used to separate the  
41 liposomes from the octanol droplet population. As illustrated in Fig. 1B, the mechanism is based  
42 on a difference in flow velocity in the channel due to shearing of the liposomes. Throughout their  
43 travel to the step in channel height, the membranes are susceptible to small disruptions due to  
44 shear. The disruptions can lead to shrinking and separation of the liposomes. This spread in  
45 liposome size is illustrated in Fig. S2 (ESI). The gradient of the curve that the scatter points lie on  
46 is a result of the fact that our optical measurement is not a confocal measurement. The fluorescent  
47  
48  
49  
50  
51  
52  
53  
54  
55  
56  
57  
58  
59  
60

1  
2  
3 drug solute surrounding smaller liposomes therefore leads to a lower apparent  $\Delta I$ , compared to  
4  
5 larger liposomes (for a detailed explanation, please refer to Cama et al.<sup>18</sup>). The analysis protocols  
6  
7 are hence identical to our previously established technique.  
8  
9

10 The resulting permeability coefficients of all the norfloxacin experiments performed in PBS are  
11  
12 combined in the histogram in Fig. 4. The total number of liposomes in the histogram is 1620 and  
13  
14 results in an overall average permeability coefficient of  $4.13 \pm 0.05 \times 10^{-6}$  cm/s (mean  $\pm$  std. error  
15  
16 of mean) and a median value of  $3.57 \times 10^{-6}$  cm/s. The values were obtained from 12 experiments  
17  
18 in 5 technical repeats. For the pH 5 measurement, five experiments on two technical repeats were  
19  
20 performed. An experiment is defined as a continuously acquired dataset measured from one batch  
21  
22 of liposomes produced on the microfluidic device. As described above, up to four experiments  
23  
24 were performed on one microfluidic device, by restarting the liposome production after completion  
25  
26 of one measurement. Each set of experiments performed on an individual device is defined as a  
27  
28 technical repeat.  
29  
30  
31  
32

33 The value obtained from the transport measurements matches the values previously obtained in  
34  
35 our group using the established electroformation liposome production technique.  
36  
37 Purushothaman *et al.* measured the permeability coefficient of norfloxacin through PGPC  
38  
39 liposomes (30:70 ratio) in a 5 mM phosphate buffer solution at pH 7.0 to be  $4.3 \pm 0.2 \times 10^{-6}$  cm/s<sup>19</sup>.  
40  
41 The main advantages of the on-chip OLA technique over electroformation are the high-throughput  
42  
43 liposome production and its compatibility with physiological salt concentrations. The higher  
44  
45 liposome production efficiency allows us to perform tests on 1620 liposomes here compared to the  
46  
47 138 liposomes in previous experiments using electroformation. Due to the greater efficiency of  
48  
49 vesicle formation under these conditions and the correspondingly higher number of data points,  
50  
51 we can provide a more precise estimate of the permeability coefficient than before, with the  
52  
53  
54  
55  
56  
57  
58  
59  
60

1  
2  
3 standard error of the mean lowered by over an order of magnitude compared to the results  
4  
5 previously reported<sup>19</sup> using electroformed vesicles. Furthermore, the possibility of producing  
6  
7 liposomes at physiological salt concentrations allows us to mimic the natural environment of a  
8  
9 bacterial cell more closely. Any possible remaining traces of solvent<sup>23</sup> (1-octanol, poloxamer  
10  
11 P-188) do not seem to alter the transport properties of the membrane, as seen by the similarity to  
12  
13 the previously acquired result.  
14  
15

16  
17 The scatter plots and histogram of the permeability measurements for ciprofloxacin are  
18  
19 displayed in Fig. S5 (ESI). The mean ( $\pm$  std. error of mean) permeability coefficient obtained for  
20  
21 this drug is  $4.99 \pm 0.07 \times 10^{-6}$  cm/s and the median value is  $4.8 \times 10^{-6}$  cm/s. The values are obtained  
22  
23 from 4 experiments (4 technical repeats) and a total of 960 vesicles. The higher permeability  
24  
25 coefficient of ciprofloxacin compared with norfloxacin is to be expected based on the chemical  
26  
27 structure of the respective molecules. Norfloxacin carries an ethyl group at the N-1 position, where  
28  
29 ciprofloxacin has a cyclopropyl group. This functional group is associated with higher lipophilicity  
30  
31 of the compound and therefore results in a higher permeability coefficient<sup>20</sup>.  
32  
33  
34  
35  
36  
37  
38  
39  
40  
41  
42  
43  
44  
45  
46  
47  
48  
49  
50  
51  
52  
53  
54  
55  
56  
57  
58  
59  
60

#### IV. Discussion and Conclusion

In this paper, we presented an integrated microfluidic platform for quantifying drug permeation across biomimetic membranes. We combined an on-chip liposome formation technique (OLA) with a downstream T-junction for the controlled exposure of liposomes to a drug solute. Norfloxacin and ciprofloxacin transport through biomimetic PGPC (1:3 ratio) liposomes was measured at physiological pH and salt concentrations. The measurements yielded permeability coefficients of  $4.13 \pm 0.05 \times 10^{-6}$  cm/s (mean  $\pm$  std. error of mean) with a median value of  $3.57 \times 10^{-6}$  cm/s for norfloxacin and  $4.99 \pm 0.07 \times 10^{-6}$  cm/s (mean  $\pm$  std. error of mean) and a median value of  $4.8 \times 10^{-6}$  cm/s for ciprofloxacin. These values are in good agreement with previous measurements<sup>19,20</sup>. We produced PGPC (1:3) liposomes to mimic the anionic charge density typically associated with bacterial membranes<sup>25–28</sup>, and used this as a model system to quantify passive drug transport through the lipid bilayer component of the Gram-negative cell envelope.

Since our method directly quantifies the permeability coefficient of the drug across the specific membrane of interest, our technique offers an alternative to traditional drug transport assays such as octanol-partition coefficients, or the parallel artificial membrane permeability assay (PAMPA) which suffer from multiple drawbacks<sup>34,35</sup>. Our method also profits from recent advances in the development of fluorescent antibiotics, as these provide another potential tool for studying and understanding drug transport processes that will lead to further insight into drug-membrane interactions<sup>36</sup>. Importantly, thanks to the microfluidic character of our method, we require only very small reagent volumes in the microliter range for our measurements<sup>37</sup>.

Another advantage of the integrated on-chip technique presented here over our previously published optofluidic permeability assay lies in the benefits of controlling liposome formation with



1  
2  
3 OLA. OLA allows the formation of large numbers of liposomes with physiological salt  
4 concentrations and with complex lipid mixtures. Other techniques such as electroformation suffer  
5 from very low yields in this environment<sup>15</sup>, or in the case of other microfluidic techniques, require  
6 extensive procedures to remove oil remnants associated with the production<sup>17</sup>. Moreover, OLA  
7 allows for the efficient encapsulation of desired solutes inside the vesicles upon production<sup>17,27</sup>.  
8 This makes it an interesting technique for biosensor-based approaches to detect drug molecules.  
9  
10 The encapsulation approach has successfully been performed by Kuhn *et al.* to measure  
11 tetracycline transport across lipid bilayers<sup>38</sup>. However, their experiments were performed using  
12 populations of small unilamellar vesicles (SUVs) of under 200 nm in radius, whereas we can work  
13 with GUVs and analyze drug transport on the single vesicle level.  
14  
15  
16  
17  
18  
19  
20  
21  
22  
23  
24  
25

26 Furthermore, the microfluidic platform presented here is not bound to a specific form of  
27 visualization such as fluorescence. Since the optics and the microfluidics are decoupled from one  
28 another, the platform can be combined with different approaches of label-free drug visualization,  
29 which is a field in its own right with various different methods published<sup>39–42</sup>. Our platform may  
30 offer the opportunity to study non-fluorescent molecules in the future.  
31  
32  
33  
34  
35  
36  
37

38 While passive diffusion across lipids is an important element in bacterial drug uptake, it is known  
39 that porin-mediated uptake plays a crucial role in drug permeation across the outer membrane<sup>7,21</sup>.  
40 Mutations of membrane proteins have furthermore been associated with antibiotic resistance<sup>21,43</sup>.  
41 The incorporation of these protein channels into liposomal membranes is an attractive target for  
42 the study of drug uptake<sup>7</sup>. However, to integrate this with on-chip liposome formation requires the  
43 development of on-chip protein reconstitution techniques, which are still pending. The successful  
44 insertion of the pore forming toxin  $\alpha$ -hemolysin into the membrane of OLA generated liposomes<sup>17</sup>  
45 suggests that the microfluidic platform can be extended to form and study more complex lipid  
46  
47  
48  
49  
50  
51  
52  
53  
54  
55  
56  
57  
58  
59  
60

1  
2  
3 compositions and even proteoliposomes on chip, potentially offering an alternative to current  
4  
5 reconstitution techniques<sup>44</sup>.  
6  
7  
8  
9  
10  
11  
12  
13  
14  
15  
16  
17  
18  
19  
20  
21  
22  
23  
24  
25  
26  
27  
28  
29  
30  
31  
32  
33  
34  
35  
36  
37  
38  
39  
40  
41  
42  
43  
44  
45  
46  
47  
48  
49  
50  
51  
52  
53  
54  
55  
56  
57  
58  
59  
60

## Associated Content

Complete experimental data set, details on the MATLAB analysis and the spread of liposome radius. The MATLAB routine is available on request.

## Author Information

\* Corresponding Author: Ulrich F. Keyser, Cavendish Laboratory, University of Cambridge, JJ Thomson Avenue, CB3 0HE, Cambridge, UK; Email: [ufk20@cam.ac.uk](mailto:ufk20@cam.ac.uk)

## Acknowledgements

MS is funded by the Friedrich-Naumann-Foundation for Freedom, JC acknowledges funding from the BBSRC and from a Wellcome Trust Institutional Strategic Support Award to the University of Exeter (204909/Z/16/Z). KAN acknowledges support from an EPSRC CASE award with the National Physical Laboratory, Winton Programme for the Physics of Sustainability, Trinity-Henry Barlow Scholarship and the ERC. DS is funded by the Winton Programme for the Physics of Sustainability and the EPSRC. KJ was supported by the Erasmus Plus student exchange programme. SD and CD acknowledge support from the ERC Advanced grants SynDiv (no. 669598) and the Netherlands Organisation for Scientific Research (NWO/OCW), as part of the Frontiers of Nanoscience program. UFK acknowledges support from an ERC consolidator grant (Designer- Pores 647144).

## References

- (1) McKenna, M. Antibiotic Resistance: The Last Resort. *Nature* **2013**, *499* (7459), 394–396.
- (2) ECDC2016. *ECDC: SURVEILLANCE REPORT. Surveillance of Antimicrobial Resistance in Europe 2016*; Stockholm, 2016.
- (3) Blair, J. M. A.; Webber, M. A.; Baylay, A. J.; Ogbolu, D. O.; Piddock, L. J. V. Molecular Mechanisms of Antibiotic Resistance. *Nat. Rev. Microbiol.* **2015**, *13* (1), 42–51.
- (4) Silver, L. L. A Gestalt Approach to Gram-Negative Entry. *Bioorg. Med. Chem.* **2016**, *24* (24), 6379–6389.
- (5) Pagès, J.-M.; James, C. E.; Winterhalter, M. The Porin and the Permeating Antibiotic: A Selective Diffusion Barrier in Gram-Negative Bacteria. *Nat. Rev. Microbiol.* **2008**, *6* (12), 893–903.
- (6) Six, D. A.; Krucker, T.; Leeds, J. A. Advances and Challenges in Bacterial Compound Accumulation Assays for Drug Discovery. *Curr. Opin. Chem. Biol.* **2018**, *44*, 9–15.
- (7) Delcour, A. H. Outer Membrane Permeability and Antibiotic Resistance. *Biochim. Biophys. Acta - Proteins Proteomics* **2009**, *1794* (5), 808–816.
- (8) Barák, I.; Muchová, K. The Role of Lipid Domains in Bacterial Cell Processes. *Int. J. Mol. Sci.* **2013**, *14* (2), 4050–4065.
- (9) Fenz, S. F.; Sengupta, K. Giant Vesicles as Cell Models. *Integr. Biol.* **2012**, *4* (9), 982.
- (10) Sercombe, L.; Veerati, T.; Moheimani, F.; Wu, S. Y.; Sood, A. K.; Hua, S. Advances and Challenges of Liposome Assisted Drug Delivery. *Front. Pharmacol.* **2015**, *6*, 286.

- 1  
2  
3 (11) Deshpande, S.; Spoelstra, W. K.; van Doorn, M.; Kerssemakers, J.; Dekker, C. Mechanical  
4 Division of Cell-Sized Liposomes. *ACS Nano* **2018**, *12* (3), 2560–2568.  
5  
6  
7  
8 (12) Xu, C.; Hu, S.; Chen, X. Artificial Cells: From Basic Science to Applications. *Mater. Today*  
9 **2016**, *19* (9), 516–532.  
10  
11  
12  
13 (13) Göpfrich, K.; Platzman, I.; Spatz, J. P. Mastering Complexity: Towards Bottom-up  
14 Construction of Multifunctional Eukaryotic Synthetic Cells. *Trends Biotechnol.* **2018**, *36*  
15 (9), 938–951.  
16  
17  
18  
19 (14) Akbarzadeh, A.; Rezaei-Sadabady, R.; Davaran, S.; Joo, S. W.; Zarghami, N.; Hanifehpour,  
20 Y.; Samiei, M.; Kouhi, M.; Nejati-Koshki, K. Liposome: Classification, Preparation, and  
21 Applications. *Nanoscale Res. Lett.* **2013**, *8* (1), 102.  
22  
23  
24  
25 (15) van Swaay, D.; DeMello, A. Microfluidic Methods for Forming Liposomes. *Lab Chip* **2013**,  
26 *13* (5), 752.  
27  
28  
29  
30 (16) Teh, S.-Y.; Khnouf, R.; Fan, H.; Lee, A. P. Stable, Biocompatible Lipid Vesicle Generation  
31 by Solvent Extraction-Based Droplet Microfluidics. *Biomicrofluidics* **2011**, *5* (4), 044113.  
32  
33  
34  
35 (17) Deshpande, S.; Caspi, Y.; Meijering, A. E. C.; Dekker, C. Octanol-Assisted Liposome  
36 Assembly on Chip. *Nat. Commun.* **2016**, *7*, 10447.  
37  
38  
39  
40 (18) Cama, J.; Chimere, C.; Pagliara, S.; Javer, A.; Keyser, U. F. A Label-Free Microfluidic  
41 Assay to Quantitatively Study Antibiotic Diffusion through Lipid Membranes. *Lab Chip*  
42 **2014**, *14* (13), 2303–2308.  
43  
44  
45  
46 (19) Purushothaman, S.; Cama, J.; Keyser, U. F. Dependence of Norfloxacin Diffusion across  
47 Bilayers on Lipid Composition. *Soft Matter* **2016**, *12* (7), 2135–2144.  
48  
49  
50  
51  
52  
53  
54  
55  
56  
57  
58  
59  
60

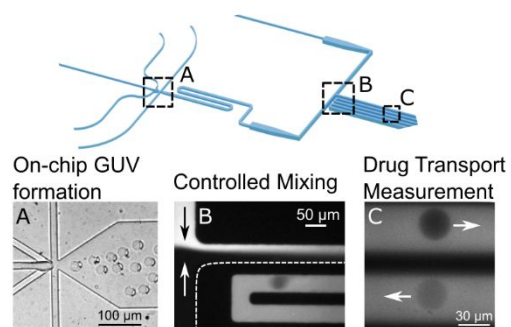
- 1  
2  
3 (20) Cama, J.; Schaich, M.; Al Nahas, K.; Hernández-Ainsa, S.; Pagliara, S.; Keyser, U. F. Direct  
4 Optofluidic Measurement of the Lipid Permeability of Fluoroquinolones. *Sci. Rep.* **2016**, *6*  
5 (1), 32824.  
6  
7  
8  
9  
10 (21) Cama, J.; Bajaj, H.; Pagliara, S.; Maier, T.; Braun, Y.; Winterhalter, M.; Keyser, U. F.  
11 Quantification of Fluoroquinolone Uptake through the Outer Membrane Channel OmpF of  
12 Escherichia Coli. *J. Am. Chem. Soc.* **2015**, *137* (43), 13836–13843.  
13  
14  
15  
16  
17 (22) Stein, H.; Spindler, S.; Bonakdar, N.; Wang, C.; Sandoghdar, V. Production of Isolated  
18 Giant Unilamellar Vesicles under High Salt Concentrations. *Front. Physiol.* **2017**, *8*, 63ss.  
19  
20  
21  
22 (23) Deshpande, S.; Dekker, C. On-Chip Microfluidic Production of Cell-Sized Liposomes. *Nat.*  
23 *Protoc.* **2018**, *13* (5), 856–874.  
24  
25  
26  
27 (24) Edelstein, A. D.; Tsuchida, M. A.; Amodaj, N.; Pinkard, H.; Vale, R. D.; Stuurman, N.  
28 Advanced Methods of Microscope Control Using MManager Software. *J. Biol. Methods*  
29 **2014**, *1* (2), 10.  
30  
31  
32  
33 (25) Ryadnov, M. G.; Mukamolova, G. V.; Hawrani, A. S.; Spencer, J.; Platt, R. RE Coil: An  
34 Antimicrobial Peptide Regulator. *Angew. Chemie Int. Ed.* **2009**, *48* (51), 9676–9679.  
35  
36  
37 (26) Vecchiarelli, A. G.; Li, M.; Mizuuchi, M.; Mizuuchi, K. Differential Affinities of MinD and  
38 MinE to Anionic Phospholipid Influence Min Patterning Dynamics in Vitro. *Mol.*  
39 *Microbiol.* **2014**, *93* (3), 453–463.  
40  
41  
42  
43 (27) Rakowska, P. D.; Jiang, H.; Ray, S.; Pyne, A.; Lamarre, B.; Carr, M.; Judge, P. J.; Ravi, J.;  
44 M. Gerling, U. I.; Kokschi, B.; et al. Nanoscale Imaging Reveals Laterally Expanding  
45 Antimicrobial Pores in Lipid Bilayers. *Proc. Natl. Acad. Sci.* **2013**, *110* (22), 8918–8923.  
46  
47  
48  
49  
50  
51  
52  
53  
54  
55  
56  
57  
58  
59  
60

- 1  
2  
3 (28) Al Nahas, K.; Cama, J.; Schaich, M.; Hammond, K.; Deshpande, S.; Dekker, C.; Ryadnov,  
4 M. G.; Keyser, U. F. A Microfluidic Platform for the Characterisation of Membrane Active  
5 Antimicrobials. *Lab Chip* **2019**, *19* (5), 837–844.  
6  
7  
8  
9  
10  
11 (29) McIntyre, J. C.; Sleight, R. G. Fluorescence Assay for Phospholipid Membrane Asymmetry.  
12 *Biochemistry* **1991**, *30* (51), 11819–11827.  
13  
14  
15  
16 (30) Ohmann, A.; Li, C.-Y.; Maffeo, C.; Al Nahas, K.; Baumann, K. N.; Göpfrich, K.; Yoo, J.;  
17 Keyser, U. F.; Aksimentiev, A. A Synthetic Enzyme Built from DNA Flips 107 Lipids per  
18 Second in Biological Membranes. *Nat. Commun.* **2018**, *9* (1), 2426.  
19  
20  
21  
22  
23  
24 (31) Nikaido, H.; Thanassi, D. G. Penetration of Lipophilic Agents with Multiple Protonation  
25 Sites into Bacterial Cells: Tetracyclines and Fluoroquinolones as Examples. *Antimicrob.*  
26 *Agents Chemother.* **1993**, *37* (7), 1393–1399.  
27  
28  
29  
30  
31  
32 (32) Uivarosi, V. Metal Complexes of Quinolone Antibiotics and Their Applications: An  
33 Update. *Molecules* **2013**, *18* (9), 11153–11197.  
34  
35  
36  
37 (33) Yang, N. J.; Hinner, M. J. Getting Across the Cell Membrane: An Overview for Small  
38 Molecules, Peptides, and Proteins. *Methods Mol. Biol.* **2015**, *1266*, 29–53.  
39  
40  
41  
42 (34) Avdeef, A.; Bendels, S.; Di, L. i.; Faller, B.; Kansy, M.; Sugano, K.; Yamauchi, Y.  
43 PAMPA—critical Factors for Better Predictions of Absorption. *J. Pharm. Sci.* **2007**, *96*  
44 (11), 2893–2909.  
45  
46  
47  
48  
49  
50 (35) Galinis-Luciani, D.; Nguyen, L.; Yazdanian, M. Is PAMPA a Useful Tool for Discovery?  
51 *J. Pharm. Sci.* **2007**, *96* (11), 2886–2892.  
52  
53  
54  
55 (36) Stone, M. R. L.; Butler, M. S.; Phetsang, W.; Cooper, M. A.; Blaskovich, M. A. T.  
56  
57  
58  
59  
60

- 1  
2  
3 Fluorescent Antibiotics: New Research Tools to Fight Antibiotic Resistance. *Trends*  
4 *Biotechnol.* **2018**, *36* (5), 523–536.  
5  
6  
7  
8  
9 (37) Streets, A. M.; Huang, Y. Chip in a Lab: Microfluidics for next Generation Life Science  
10 Research. *Biomicrofluidics* **2013**, *7* (1), 011302.  
11  
12  
13  
14 (38) Kuhn, P.; Eyer, K.; Allner, S.; Lombardi, D.; Dittrich, P. S. A Microfluidic Vesicle  
15 Screening Platform: Monitoring the Lipid Membrane Permeability of Tetracyclines. *Anal.*  
16 *Chem.* **2011**, *83* (23), 8877–8885.  
17  
18  
19  
20  
21 (39) Zeng, J.; Eckenrode, H. M.; Dounce, S. M.; Dai, H.-L. Time-Resolved Molecular Transport  
22 across Living Cell Membranes. *Biophys. J.* **2013**, *104* (1), 139–145.  
23  
24  
25  
26  
27 (40) Nguyen, T. T.; Rembert, K.; Conboy, J. C. Label-Free Detection of Drug-Membrane  
28 Association Using Ultraviolet–Visible Sum-Frequency Generation. *J. Am. Chem. Soc.*  
29 **2009**, *131* (4), 1401–1403.  
30  
31  
32  
33  
34 (41) Custódio, J. B.; Almeida, L. M.; Madeira, V. M. A Reliable and Rapid Procedure to  
35 Estimate Drug Partitioning in Biomembranes. *Biochem. Biophys. Res. Commun.* **1991**, *176*  
36 (3), 1079–1085.  
37  
38  
39  
40  
41  
42 (42) Fox, C. B.; Horton, R. A.; Harris, J. M. Detection of Drug–Membrane Interactions in  
43 Individual Phospholipid Vesicles by Confocal Raman Microscopy. *Anal. Chem.* **2006**, *78*  
44 (14), 4918–4924.  
45  
46  
47  
48  
49  
50 (43) Watanabe, T. Infective Heredity of Multiple Drug Resistance in Bacteria. *Bacteriol. Rev.*  
51 **1963**, *27*, 87–115.  
52  
53  
54  
55 (44) Jørgensen, I. L.; Kemmer, G. C.; Pomorski, T. G. Membrane Protein Reconstitution into  
56  
57  
58  
59  
60



1  
2  
3 Giant Unilamellar Vesicles: A Review on Current Techniques. *Eur. Biophys. J.* **2017**, 46  
4  
5  
6 (2), 103–119.  
7  
8  
9  
10  
11  
12  
13  
14  
15  
16  
17  
18  
19

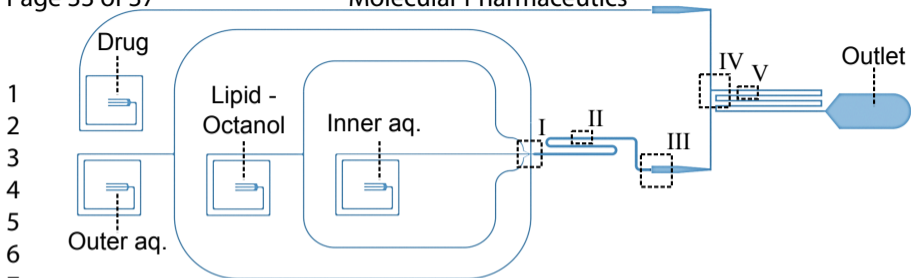


For Table of Contents Only

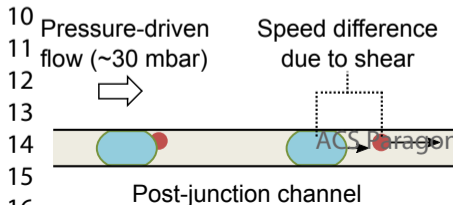
# A Microfluidic Chip Schematic

Page 33 of 37

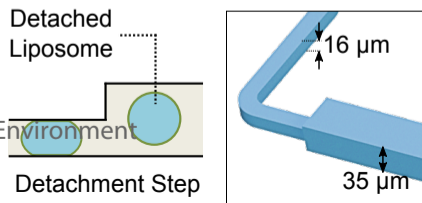
Molecular Pharmaceuticals



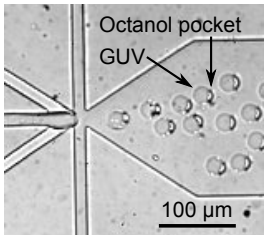
## B Separation of Octanol Droplets (II)



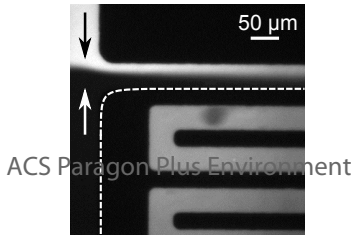
## C Surface Detachment of Liposomes (III)



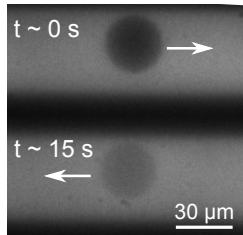
# A Liposome Production



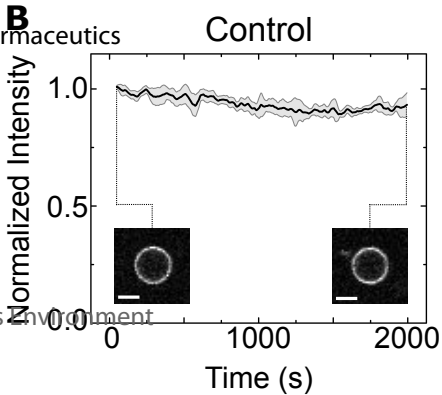
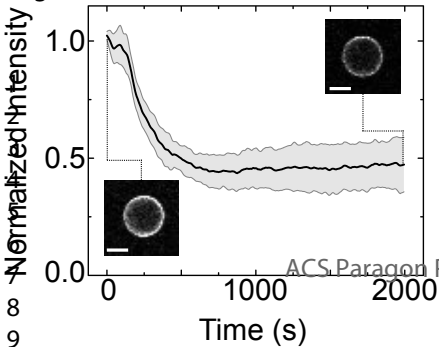
# B Controlled Molecular Pharmaceutics Mixing



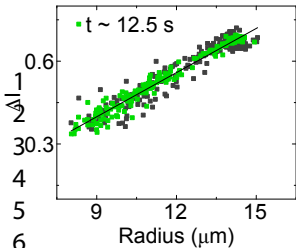
# C Transport Measurement



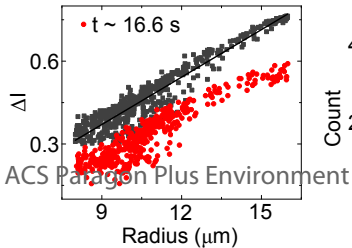
1  
2  
3  
4  
5  
6  
7



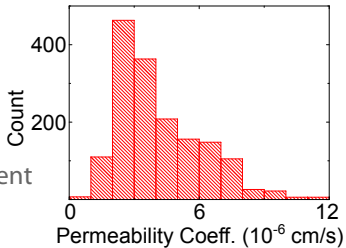
pH 5

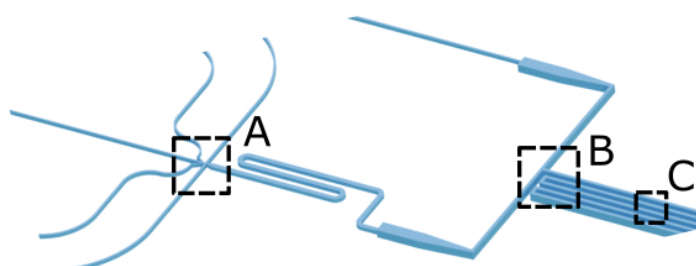


Molecular PA (PBS) deuterics

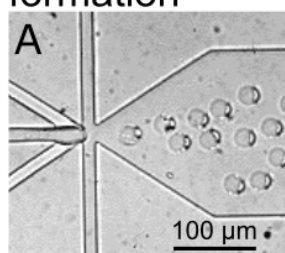


Histogram of Permeability Coeff. ( $10^{-6}$  cm/s)

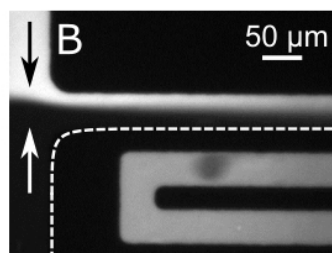




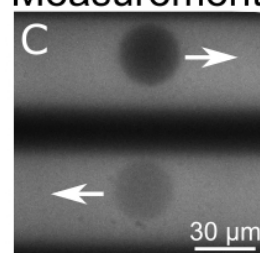
On-chip GUV formation



Controlled Mixing



Drug Transport Measurement



For Table of Contents Only

68x44mm (300 x 300 DPI)